

CFCI FINAL REPORT

Introduction

The discovery and understanding of new, improved materials to advance fuel cell technology are the objectives of the **Cornell Fuel Cell Institute (CFCI)** research program. CFCI was initially formed in 2003. This report highlights the accomplishments from 2006-2009.

Many of the grand challenges in energy science and technology are based on the need for materials with greatly improved or even revolutionary properties and performance.¹⁻⁶ This is certainly true for fuel cells, which have the *promise* of being highly efficient in the conversion of chemical energy to electrical energy. Fuel cells offer the possibility of efficiencies perhaps up to 90 % based on the free energy of reaction.

Thus, there is considerable interest in fuel cells which, however, have yet to live up to their promise, not only for efficiency, but also for cost, durability, performance, etc.⁷⁻¹² Here, the challenges are clearly in the materials used to construct the heart of the fuel cell: the membrane electrode assembly (MEA). The MEA consists of two electrodes separated by an ionically conducting membrane. Each electrode is a nanocomposite of electronically conducting catalyst support, ionic conductor and open porosity, that together form three percolation networks that must connect to each catalyst nanoparticle; otherwise the catalyst is inactive.

While there are a number of different fuel cell technologies^{12, 13}, the CFCI is **focused on polymer electrolyte membrane fuel cells (PEMFCs)**. The broadest applications of these fuel cells in portable power or individual transportation vehicles. The highest interest is in fuels that are carbon neutral, such as hydrogen, which could be carbon neutral if it is generated from sunlight, rather than from natural gas, as is done now. Fuels derived from algal or plant matter are also of interest, if we could discover catalysts that enable complete oxidation of those fuels, or if they could be efficiently converted to hydrogen.

Our research program is divided into four main areas: Electrocatalysts and Supports, Self-Assembly and Meso-Structured Electrodes, Membranes and Theory. The first section is further sub-divided into combinatorial synthesis and screening, oxide supports, mechanistic studies and surface characterization. This report highlights selected advances rather than give an exhaustive account of previous results. A full appreciation of the scope and advances of our program can be garnered from our publications¹⁴⁻⁸¹

Electrocatalysts and Supports

A. Development of Combinatorial Synthesis and Screening Methods for Catalyst Discovery:

We have continued our extensive use of combinatorial methods in the search for enhanced electrocatalytic activity for fuel cell applications. We identify and characterize new catalysts through analysis of composition-spread thin films (generated by sputtering of up to five elements onto a conducting substrate). The entire substrate can then be screened for electrocatalytic activity using a rapid fluorescence assay to discover which point in the film is most active.^{13, 15, 38, 50}

We have carried out extensive studies in which we have looked at a wide variety of binary and ternary combinations of metals (initially, with Pt as one of the components). To date, over five hundred composition spread films have been tested and fluorescence onset potentials (which serve as an initial indicator of electrocatalytic activity) determined. For example, Figure 1 presents a range of ternary Pt-A-B composition spreads tested for methanol oxidation. As is evident from the main figure and the accompanying histogram, there are a number of

combinations that appear especially attractive with onset potentials for methanol oxidation as low as -300 mV (vs. Ag/AgCl). We have also developed an analysis program that allows the fluorescence to be mapped onto a ternary phase diagram, thus facilitating data mining.

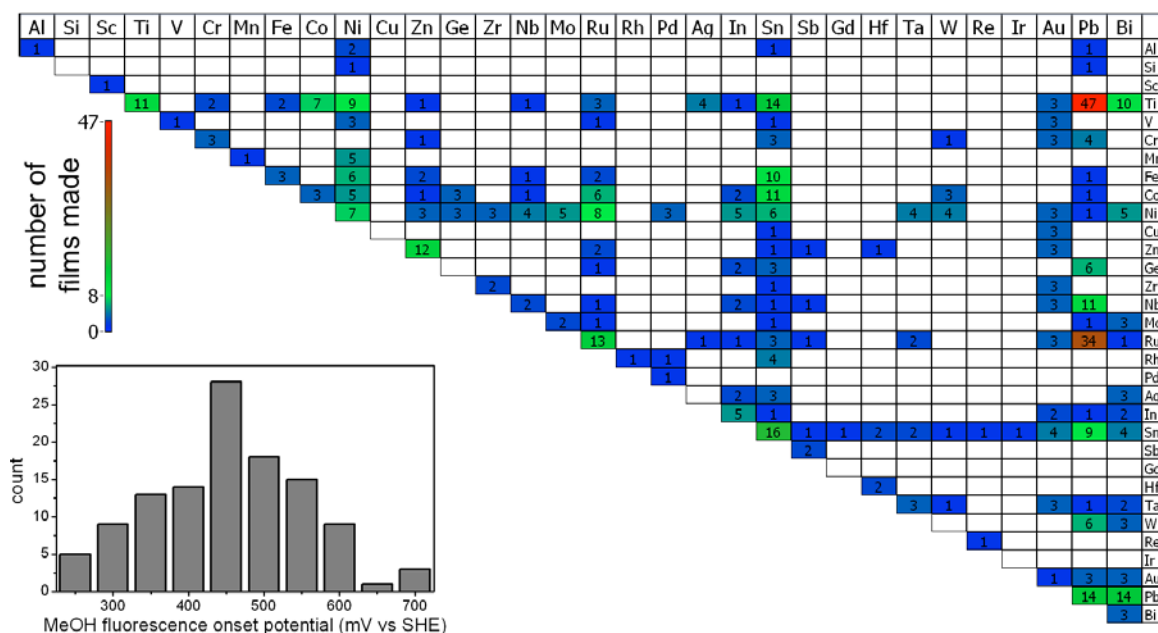


Figure 1: Summary map of Pt-A-B (A= columns, B= rows) ternary compositions for methanol oxidation with the numbers corresponding to the number of composition spreads made of the particular combination of elements. For the set of chemical systems active for methanol oxidation, the inset shows a histogram of the fluorescence onset potential at the most active point in the binary or ternary system.

One of the challenges in the effective use of results from combinatorial searches is trying to establish which parameter(s) might be responsible for the observed behavior. In trying to

rationalize such results we have found some approaches that appear especially attractive and promising.

For example, Figure 2 presents a plot of fluorescence-determined half-wave potentials for ethanol oxidation as a function of the fraction of X ion PtX alloy materials as well as the dependence of the onset potential of binary phases for ethanol oxidation as a function of the Pauling electronegativity parameter and % change in lattice parameter at 50% or at the solubility limit. From such plots one can begin to establish the importance of such parameters on electrocatalytic activity.

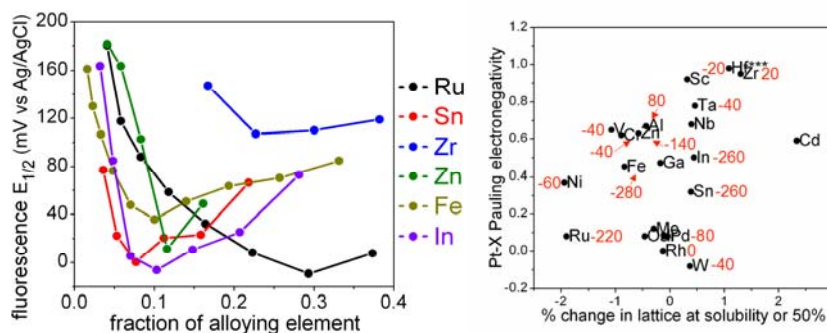


Figure 2: (Left) Plot of fluorescence-determined half-wave potential for ethanol oxidation as a function of the fraction of X in PtX alloy materials. (Right) The difference in Pauling electronegativities of Pt and element X (denoted at each point) plotted versus the percent change in lattice constant at element X's solubility in Pt (or at 50% for some cases). The red values correspond to the respective ethanol fluorescence onset potentials at the most active point in the binary system.

From such plots one can begin to establish the importance of such parameters on electrocatalytic activity.

Making use of such an analysis as well as compositional information from the combinatorial libraries, it appeared that a Pt/Sn composition of ca. 90/10 should have very attractive properties as an electrocatalyst. This was, in fact, borne out by experiment as seen in Figure 3, where the optimal Pt/Sn alloy is better than the optimal Pt/Ru alloy for the oxidation of ethylene glycol and ethanol. We have not yet established if the oxidation of these fuels is complete. Theoretical work to understand the origin of this behavior is currently underway. This also suggests that one may be able to customize a catalyst for a particular fuel.

Another critical parameter to consider is the difference between the geometric surface area and the specific surface area of the composition spread film. The difference has to do with the roughness of some regions of a fraction of composition spread films and the accessibility of fuel to the surface. In a recent publication, we showed that PtZn exhibits a shift in onset potential of over 300 mV with differing film thicknesses.³⁴ Bulk leaching (oxidation and dissolution of one component) of Zn from some parts of the composition spread film gives rise to an increase in specific surface area and thus a shift in the apparent onset potential. To account for this change in surface structure, a test was developed using a ferrocene redox couple (fast, stable, transport limited, 1-electron process) to probe the surface and enable

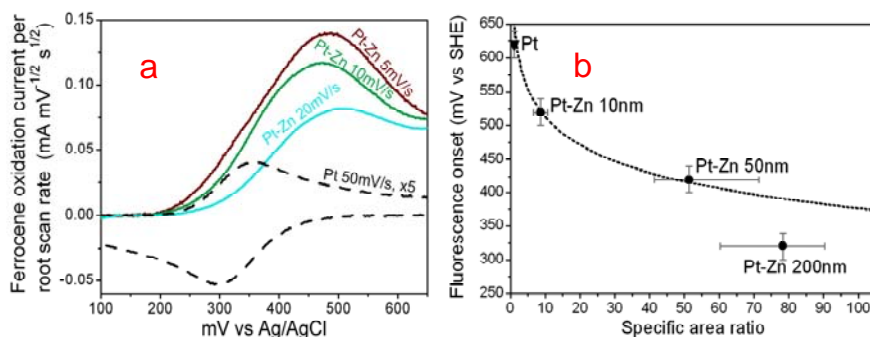


Figure 4a. Measured ferrocene redox currents, scaled by the square root of the sweep rate, plotted for different thin-film electrodes using the same geometric area. The cyclic voltammogram (dotted line) acquired at 50 mV/s on a planar Pt film is scaled by a factor of 5. The forward scans (ferrocene oxidation waves) are shown for three scan rates with a porous 200 nm Pt-Zn film. The systematic decrease in peak height with increasing scan rate reflects the fine pore structure of the film. b. The Pt-Zn fluorescence onset potential is shown as a function of the specific surface area ratio measured by the ferrocene linear sweep voltammetry technique. For comparison, the fluorescence onset potential of a planar Pt film is shown at unity surface area ratio.

the surface area to be calculated. In Figure 4, the ferrocene voltammograms of differing PtZn thicknesses are depicted and the values of the onset potentials versus specific surface area are shown. Thus, with the use of the redox couple, we can provide a more thorough comparison of surface area of composition spreads that contain metals that can be leached at high anodic potentials. Since leaching behavior at temperatures well below the melting point of the metals is largely determined by kinetic factors, there is a large difference between surface and bulk leaching behavior.⁸²⁻⁹² Surface leaching from the first few monolayers can occur at potentials quite negative (perhaps 300 – 400 mV) of the standard reduction potential for that metal since the bulk concentration of the ion in solution is essentially zero. This fact is commonly exploited to prepare “core-shell” nanoparticles. Bulk leaching occurs only when the concentration of the second metal is above 50 % or so⁸²⁻⁹², an

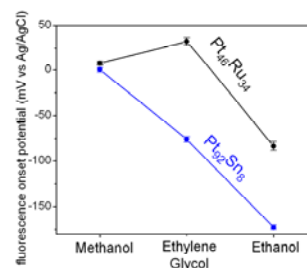


Figure 3. Fluorescence onset potential plotted versus fuel tested for two thin film catalysts (Pt₄₆Ru₃₄ and Pt₉₂Sn₈). Pt₉₂Sn₈ shows a significant drop in onset potential when tested with different fuels compared to Pt₄₆Ru₃₄.

the surface area to be calculated. In Figure 4, the ferrocene voltammograms of differing PtZn thicknesses are depicted and the values of the onset potentials versus specific surface area are shown. Thus, with the use of the redox couple, we can provide a more thorough comparison of surface area of composition spreads that contain metals that can be leached at high anodic potentials. Since leaching behavior at

expectation that we have verified in many composition spread films. Large changes in surface area (factors up to 100!) are expected, and found, when bulk leaching occurs. On the other hand, changes in electrode surface area with surface leaching are much smaller (factors of 2 or 3).

C. Oxides as supports and catalysts:

As is now widely appreciated, the carbon black catalyst support employed in fuel cells corrodes too rapidly, especially under transient load and on/off operating conditions.^{7,8,11,12} Even losses of 5% can cause a dramatic, sometimes catastrophic, degradation of performance. Carbon, in any form, is thermodynamically stable below about +0.2 V, but only kinetically stable above that ($C + 2 H_2O \rightarrow CO_2 + 4 H^+ + 4 e^-$, $E^0 = 0.207 V$). However, under fuel starvation conditions in a fuel cell stack, even the anode of a single cell can be forced to high potentials (up to + 1.5 V) as oxidation of the carbon is the only process that can support the imposed stack current.⁸ In fact, no single element is thermodynamically stable at such potentials in acidic aqueous media.⁹³

If stability (or sufficient metastability) in air/water is desired, then one should look to oxides in which metals are already near or in their highest oxidation state. Materials based on other anions, such as sulfides, carbides and nitrides will thermodynamically prefer to oxidize or hydrolyze to oxides at high potential. Depending on the material and conditions (pH, temperature, other ions in solution, etc.) the oxidation or hydrolysis of these other classes of materials will form surface reaction layers from a few nm thick to completely consuming the material. The key issues in considering oxides for cathode catalyst supports are: (1) structural and electronic (meta)stability of the bulk as well as the surface at the potentials and pH of use, and (2) bulk and surface electronic conductivity. There are so few binary oxides that are insoluble at low pH and high potential that they can be listed: TiO_2 , Nb_2O_5 , Ta_2O_5 and WO_3 .⁹³ Hydrated forms of these oxides, prepared from aqueous solution, may be less stable at certain pHs or potentials^{93,94}, but we consider here the more stable structures, such as the rutile form of TiO_2 . While none of the above oxides is electronically conducting, a conductivity of 0.1 S/cm is all that is needed for catalyst supports.¹¹ We also anticipate that oxide supports can interact synergistically with the catalyst to improve catalyst performance, as has been observed for NbO_2 .⁹⁵

Based on the high stability of TiO_2 in water over a broad range of pH (-1 to 14) and from low to high potential (the actual range is pH dependent), as indicated by the Pourbaix diagrams⁹³, and as observed in devices such as Graetzel photovoltaic cells^{96,97}, it seemed likely that some form of doped TiO_2 materials might be both electrically conducting and quite resistant to corrosion under fuel cell conditions (especially in fuel cells operating near "room temperature").⁹⁸

DiSalvo and Abruña have recently shown that W-doped TiO_2 (rutile phase: $Ti_{1-x}W_xO_2$) is conducting and, as 50 nm nano-particles, suitable as catalyst support and is "stable" in oxidizing acids for over a year (publications in preparation). Even at pH = 11 (in NH_4OH and in air) the 50 nm particles do not dissolve nor oxidize. While we will also examine Nb_2O_5 , Ta_2O_5 and WO_3 as doping hosts for catalyst supports, they are more difficult to dope to the metallic state while maintaining the host structure (at least at high temperatures). They also have more open structures, perhaps allowing easier access to water or H^+ , as in H_xWO_3 . While we will explore all these systems, for discussion purposes, we focus here only on TiO_2 as a host.

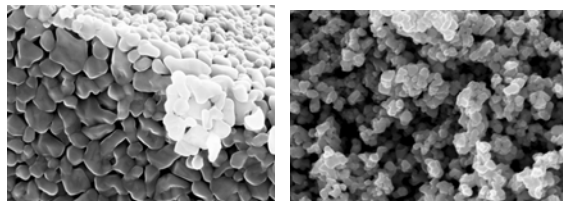


Figure 5: Images of (left) Phase pure rutile $Ti_{1-x}W_xO_2$ particles and (right) Low magnification image showing uniformity of bulk.

It is known that rutile (TiO_2) can be doped with other cations to prepare $\text{Ti}_{1-x}\text{M}_x\text{O}_2$ where $\text{M} = \text{Zr}, \text{Hf}, \text{V}, \text{Nb}, \text{Ta}, \text{Cr}, \text{Mo}, \text{W}, \text{Ru}, \text{Os}$ and Ir . Some of the binary oxides of these metals have been studied in electrochemical environments.^{95, 99-108} In most cases, preparation of bulk powders is easily carried out under conditions that fix the oxygen stoichiometry to 2 per cation. For example, sealing the appropriate ratio of precursors in a silica tube is sufficient to fix the oxygen stoichiometry during synthesis: eg. at 1100 °C with a halide transport agent such as chlorine: $(1-x) \text{TiO}_2 + 2x/3 (0.5 \text{W} + \text{WO}_3) \rightarrow \text{Ti}_{1-x}\text{W}_x\text{O}_2$. DiSalvo has shown that the maximum doping (x_{max}) that retains the rutile structure is different for different dopants, but is typically near 50 %. At doping levels above x_{max} , either two phase mixtures or different structures (some are just distorted variants of rutile) result. Much of our testing of stability under acidic and alkaline conditions has focused on this W doped rutile, where we have found long term stability (up to 1 year so far) for x at least up to 0.5, not only in acids such as HNO_3 (the stability could be anticipated from the Pourbaix diagrams for Ti and W^{93}), but also in bases such as NH_4OH . We surmise that the TiO_2 framework imparts kinetic stability to the "trapped" doping metal oxide, at least in the case of W. These initial (meta)stability observations are indeed exciting.

We find bulk conductivity of approximately 10^2 S/cm in $\text{Ti}_{1-x}\text{W}_x\text{O}_2$ at $x = 0.3$, even though the expected percolation limit is near $x = 0.5$.¹⁰⁹ As found in preliminary DFT calculations by Hoffmann and DiSalvo¹⁸, the electrons in the occupied W 5d orbitals spread out on neighboring Ti, similar to what is seen in superlattices of $\text{LaTiO}_3/\text{SrTiO}_3$ (see later in this section).¹¹⁰ While W in $\text{Ti}_{1-x}\text{W}_x\text{O}_2$ has the formal oxidation state of W^{4+} , XPS shows that most of the W at the surface (top 1 nm) is oxidized to W^{6+} upon air exposure. The material in bulk (50 nm particles), however, remains black and conducting. We have found that the surface W^{6+} can be removed by washing with NaOH (aq), creating core-shell particles of $\text{Ti}_{1-x}\text{W}_x\text{O}_2$ with a topmost layer or two of TiO_2 . This surface appears to be sufficiently conducting due to electron tunneling from W^{4+} below the surface.

In order to synthesize the above oxides as nano-particles (30 to 50 nm needed for supports), a low temperature synthesis method is needed. Sol-gel techniques are widely used for the synthesis of nano-scale mixed-metallic oxides. The nanometer-scale mixing of precursors enables the use of lower calcination temperatures, allowing homogeneous products to form without significant grain or particle size growth. Using sol-gel techniques, we have prepared $\text{Ti}_{(1-x)}\text{W}_x\text{O}_2$ and characterized the resulting materials via SEM, microprobe analysis, and XRD. One successful procedure is as follows: (1) dissolve titanium(IV) isopropoxide and tungsten (VI) isopropoxide in diglyme and add citric acid and glycol, (2) heat in air to 160 °C to produce a white powder, (3) calcine the resulting powder at 350-450 °C for 10-50 hrs and finally (4) heat in a sealed silica tube to 750 °C for 24h with Zr foil to reduce W(VI) to W(IV) . This results in the

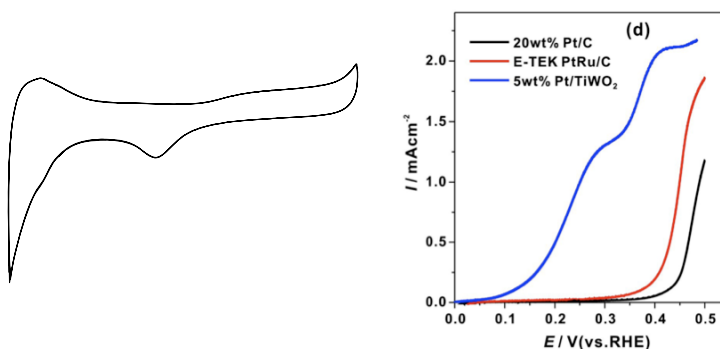


Figure 6 (a) Cyclic Voltammetry of $\text{Pt/Ti}_{0.7}\text{W}_{0.3}\text{O}_2$ coated GC electrode in 1 M H_2SO_4 (b) Hydrogen Oxidation on $\text{Pt/Ti}_{0.7}\text{W}_{0.3}\text{O}_2$ coated GC electrode in 0.1 M H_2SO_4 .

synthesis of phase pure rutile $Ti_{1-x}W_xO_2$. (Fig 5) The X-ray domain sizes were estimated to be about 30- 40 nm from XRD line widths, while the SEM indicated particle sizes from 30 to 100 nm.

Catalyst Support Interactions

We have also carried out a preliminary electrochemical characterization of these materials. In an argon saturated 0.1M H_2SO_4 solution, $Ti_{0.7}W_{0.3}O_2$ exhibited a featureless voltammetric profile over the potential range of -0.50 to +1.50V (vs Ag/AgCl) indicating that $Ti_{0.7}W_{0.3}O_2$ shows considerable promise as a catalyst support, since it is electrically conducting, stable at low pH and stable over the potential range of interest for fuel cell operation.

Additionally, we have prepared and characterized a composite of Pt nanoparticles on $Ti_{0.7}W_{0.3}O_2$. Figure 6A shows the voltammetric profile of a rotating electrode decorated with that composite in 0.1M H_2SO_4 solution. It is evident that the response is that expected for a polycrystalline platinum electrode with hydrogen adsorption/desorption and platinum oxide formation and reduction regions clearly visible. This material exhibited a stable hydrogen oxidation current (Figure 6B) with a level of activity comparable to that of commercial Pt nanoparticle catalyst.

Catalytic Activity of Oxides

Finally, oxides themselves may be interesting catalysts, perhaps more so for oxygen reduction than fuel oxidation. There have been scattered reports of such activity in various oxides under a variety of conditions (including TiO_2 , ZrO_2 , Mo/V polyoxometallates, Mn, Co, Nb and Ta oxides, WO_3 , etc.¹¹¹⁻¹²⁰ However, some of these materials dissolve under acidic conditions. Can the appropriate metals be doped into rutile to impart physical and chemical stability under acidic conditions, maintain conductivity and also impart catalytic activity? Preliminary studies suggest that the answer is affirmative. This will open up the possibility of acidic fuel cells that contain little or no precious metals. Further, it is very likely that these same oxide materials will be quite stable in alkaline conditions, a topic we will visit later.

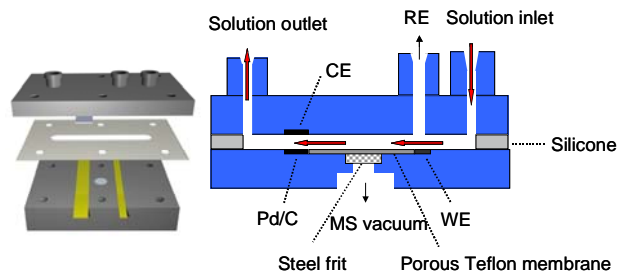


Figure 7. Schematic of channel flow dual electrode DEMS cell.

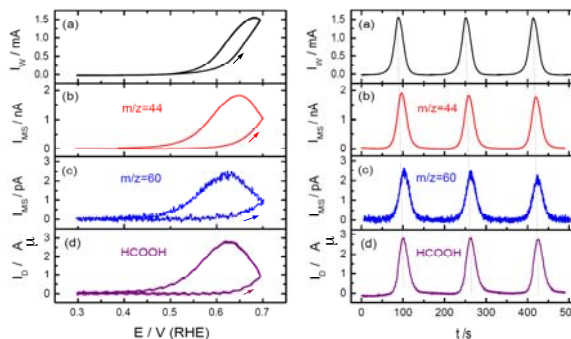


Figure 8: (Left panel) Simultaneously recorded cyclic voltammogram (a) and corresponding mass spectrometric cyclic voltammograms of CO_2 at $m/z = 44$ (b), methyl formate at $m/z = 60$ (c) and HCOOH oxidation current measured by Pd/C electrode (d). (Right panel) Currents from left panel plotted vs. time. Scan rate: 10 mV/s. Electrolyte flow rate: 12 μ L/s.

D. Mechanistic studies

An integral part of our investigations is the study of the mechanisms of oxidation of small

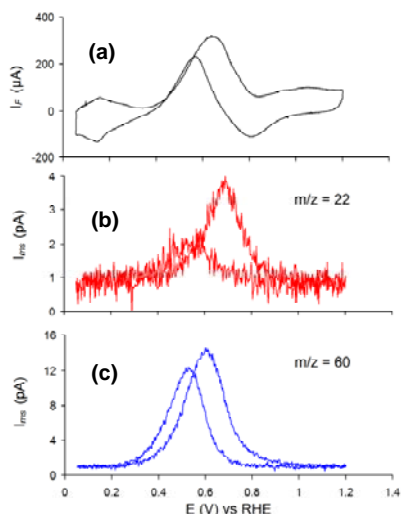


Figure 9: DEMS data for the electrooxidation of 10 mM DMM on Pt/C 50%
(a) Faradaic current, mass spectrometric cyclic voltammograms for (b) CO₂ at $m/z = 22$, and (c) methyl formate at $m/z = 60$.

organic molecules (SOMs) that can serve as potential fuels in fuel cell applications. Of particular utility and relevance has been the use of differential electrochemical mass spectrometry (DEMS).^{57, 64} This technique can provide a wealth of mechanistic information by allowing the correlation of electrochemical data with mass spectrometric analysis in-situ and in real time. However, one of the limitations of DEMS is that a number of key products/intermediates, especially in the oxidation of methanol, such as formic acid and formaldehyde, are not sufficiently volatile for DEMS determination. In an effort to mitigate this limitation, we recently⁶⁵ designed a new channel flow DEMS cell (Fig. 7) that incorporates two electrodes: a working electrode and a detecting electrode (Pd/C) that can selectively oxidize HCOOH. Between these two electrodes is a porous Teflon membrane. CO₂ and methyl formate can evaporate through the Teflon membrane into the vacuum chamber. We can use the mass spectrometer to detect CO₂ and methyl formate, and use the Pd electrode to detect formic acid. Thus, this set-up is akin to a rotating ring-disk electrode, allowing for the electrochemical detection of products generated at the first

electrode and that are not amenable to DEMS analysis.

As an example, Fig. 8 shows results for methanol oxidation at a carbon-supported Pt catalyst studied with this new cell. The left panel in figure 8 presents (a) the cyclic voltammogram, (b) the CO₂ signal measured by DEMS, (c) methyl formate generation, also detected by DEMS, and (d) the formic acid signal measured with the Pd (detecting) electrode. The right hand panel presents the results in triplicate (as a function of time) demonstrating the robustness and reproducibility of the system. After calibrating the DEMS setup, we can calculate the current efficiencies and product yields for CO₂, HCOOH, methyl formate and also HCHO, which are listed in Table 1.

In an effort to expand the range of fuels for fuel cell applications, we have carried out a study of the oxidation dimethoxymethane (DMM) on carbon-supported Pt nanoparticles (Pt/C) using electrochemistry, DEMS and FT-IR. DMM has several attractive properties for use as a fuel in direct fuel cells. Its complete oxidation to CO₂ yields 16 electrons, compared to the 12 obtainable from ethanol. It also has no C-C bonds, which are difficult to break, especially near room temperature, and lead to low efficiencies for complete oxidation to CO₂.

Products	Current efficiency (%)	Product yield (%)
CO ₂	91	81
HCOOH	2	3
HCOOCH ₃	2	3
HCHO	5	13

Table 1: Current efficiencies and product yields of CO₂, HCOOH, HCOOCH₃ and HCHO during methanol oxidation on Pt/C electrode. (WE: Pt/C [16 mg Pt / (2.5x6) mm²]; Electrolyte: 1M methanol + 0.1M H₂SO₄; Error bar: ~±10%)

The onset for DMM oxidation is 150 to 200 mV more negative than that of methanol; though its oxidation kinetics appear to be slower. With DEMS, we have tracked the formation of CO_2 via CO_2^{++} , at $m/z = 22$ (Figure 9). The mass spectrometric cyclic voltammogram (MSCV) for CO_2 showed a 2 to 3 fold greater current in the positive going sweep relative to the negative going sweep. The additional current is likely due to oxidative stripping of adsorbates formed at low potentials.

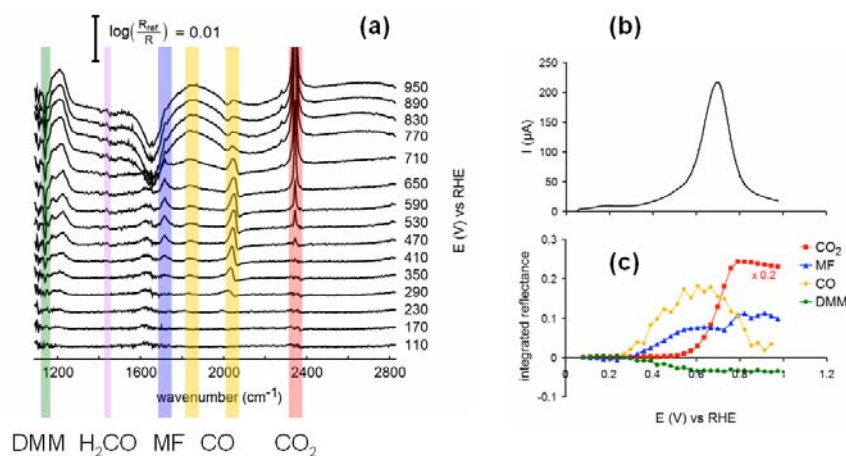


Figure 10: (a) FT-IR data for the electrooxidation of 50 mM DMM on Pt/C 50% at 1 mV/s, showing peaks for CO_2 , CO_{ads} , methyl formate (MF) and formaldehyde production as well as a peak for DMM consumption; (b) Faradaic current; (c) integrated intensities for the bands of the major products.

as adsorbates on the catalyst surface. For 10 mM DMM, current efficiencies for CO_2 production ranging from 55 to 80% were observed. The variability is likely due to differences in the residence time of partial oxidation products near the catalyst, which could vary if the distribution of particles on the surface differs. Methyl formate (MF) can be observed as an important partial oxidation product via its molecular ion, at $m/z = 60$. The MSCV for MF shows preferential production at lower potentials, and peak production about 90 mV more negative than CO_2 . The infrared spectra also show a peak at 1716 cm^{-1} , which may be attributed to the carbonyl stretch of MF. It is possible that formic acid also contributes to this peak, as its carbonyl stretch is within a few wavenumbers of that of MF. With the DEMS cell used in this work, formic acid cannot be detected directly, due to its relatively low vapor pressure. We plan to test DMM in the newly designed channel flow cell described earlier (vide-supra), and use a Pd detector electrode to determine whether formic acid is produced. A peak in the IR spectrum at 1435 cm^{-1} could indicate that formaldehyde is also formed. We feel confident that these mechanistic studies will provide most valuable insights to catalysts development.

as adsorbates on the catalyst surface.

For 10 mM DMM, current efficiencies for CO_2 production ranging from 55 to 80% were observed. The variability is likely due to differences in the residence time of partial oxidation products near the catalyst, which could vary if the distribution of particles on the surface differs.

Methyl formate (MF) can be observed as an important partial oxidation product via its molecular ion, at $m/z = 60$. The MSCV for MF shows preferential production at lower potentials, and peak production about 90 mV more negative than CO_2 . The infrared spectra also show a peak at 1716 cm^{-1} , which may be attributed to the carbonyl stretch of MF. It is possible that formic acid also contributes to this peak, as its carbonyl stretch is within a few wavenumbers of that of MF. With the DEMS cell used in this work, formic acid cannot be detected directly, due to its relatively low vapor pressure. We plan to test DMM in the newly designed channel flow cell described earlier (vide-supra), and use a Pd detector electrode to determine whether formic acid is produced. A peak in the IR spectrum at 1435 cm^{-1} could indicate that formaldehyde is also formed. We feel confident that these mechanistic studies will provide most valuable insights to catalysts development.

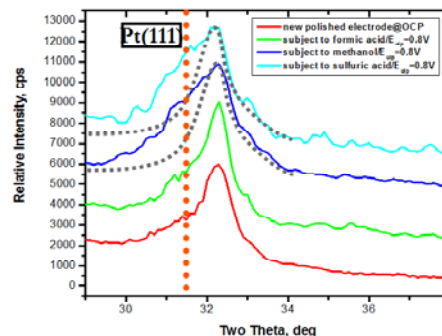


Figure 11: X-ray GID of PtBi subjected to different applied potentials.

E. Surface characterization:

Our surface characterization methods have emphasized the use of *in-situ* X-ray-based techniques and *ex-situ* ultrahigh vacuum (UHV) methods coupled with electrochemical characterization.

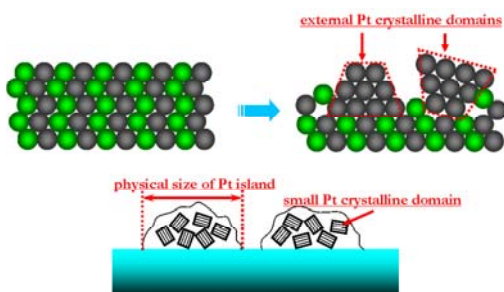


Figure 12. Scheme for formation of Pt nano-crystalline islands on PtBi surface.

+0.80~+1.0V vs. Ag/AgCl). When the potential applied to a PtBi electrode in contact with a 0.1M sulfuric acid solution was continuously increased from +0.40V to +1.20V, Bi leached out from the electrode surface. The remaining platinum atoms sintered together to form small crystalline domains on the electrode surface. A detectable Pt(111) diffraction shoulder peak was evident for potentials beyond +0.80V (Fig.11). Based on the width of the reflection and through the use of the Scherrer equation, the Pt crystalline domain was estimated to be ca. 5~8nm. Further potential cycling gave rise to some “ripening” resulting in larger Pt islands (Fig. 12). PtPb intermetallic electrodes showed very similar behavior and trends to PtBi.

When a PtBi electrode was subjected to a similar applied potential profile, but in the presence of 0.2M formic acid/0.1M sulfuric acid, Bi leaching was precluded and no detectable Pt diffraction peak was evident even at potentials as high as +1.0V. However, in the presence of 0.2M methanol/0.1M sulfuric acid, the surface degradation process (Bi-leaching and formation of platinum nanocrystals) was very similar to that in the presence of sulfuric acid alone. We believe that this behavior arises from a kinetic stabilization of the PtBi surface in the presence of molecules that can serve as fuel. For example, while PtBi is very active towards formic acid oxidation it has virtually no activity towards methanol oxidation. As a result, the oxidation of formic acid can “consume” the oxidizing equivalents generated at high applied potentials. Since the PtBi surface exhibits no catalytic activity towards methanol oxidation, the oxidizing equivalents go towards surface oxidation of PtBi with the concomitant leaching of Bi.

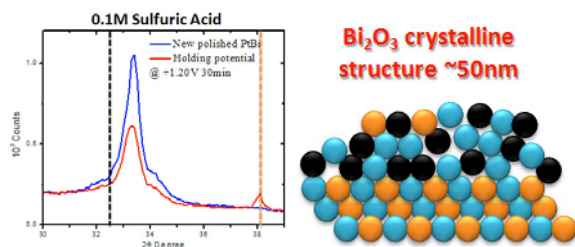


Figure 14: X-ray Grazing Incident Diffraction (GID) investigation for PtBi electrode before and after electrochemical pretreatment in 0.1M sulfuric acid. Schematic depiction of the formation of a Bi_2O_3 overlayer.

formic acid adsorbs strongly to the PtBi surface and this, in turn, stabilizes the surface. In order to test for this possibility we employed malonic acid which can be adsorbed but PtBi exhibits no electrocatalytic activity towards its oxidation. As shown in Figure 13 there was no stabilization,

X-ray based studies: As we have articulated in the past, PtM (M = Bi, Pb etc.) intermetallic compounds are very promising electrocatalysts for the oxidation of small organic molecules. In previous *ex-situ* X-ray Photoelectron Spectroscopy (XPS)¹⁹ and X-ray Grazing Incidence Diffraction (GID)⁴¹ experiments we have shown that surface composition and structure will be significantly altered as a function of the applied potential. The less noble metal (Bi or Pb) will leach out from the electrode surface and a Pt-rich surface will be formed at relatively high potentials (ca.

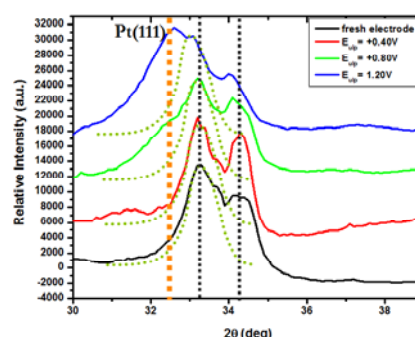


Figure 13: X-ray GID of PtBi in the presence of malonic acid.

An alternative explanation is that

malonic acid adsorbs strongly to the PtBi surface and this, in turn, stabilizes the surface. In order to test for this possibility we employed malonic acid which can be adsorbed but PtBi exhibits no electrocatalytic activity towards its oxidation. As shown in Figure 13 there was no stabilization,

indicating that this “kinetic stabilization” effect depends on the ability of the electrode surface (PtBi in the present case) to oxidize the molecule in question.

Most recently, we have carried out studies for PtBi in 0.1M H₂SO₄ in which rather than sweeping the potential, we have held the potential constant at increasingly more positive values. In this case we see no evidence of formation of Pt nanocrystals (no reflections due to Pt) but rather peaks associated with the formation of a Bi₂O₃ layer (Figure 14) which we estimate to be about 50 nm in thickness. Similar results were observed in perchloric acid, suggesting that anion adsorption is not likely to be responsible for the observed effect. It is also interesting to note that surfaces in which the Bi had been leached out (via potential scanning) vs surfaces with a Bi₂O₃ overlayer (generated by holding the potential) exhibited very similar electrocatalytic activity.

Self-Assembly and Meso-Structured Electrodes

A major challenge in fuel cell systems is the optimization of the mesoscale structure of the electrodes. In order to be electrochemically active, each catalyst particle must be connected to three interconnected percolation networks that provide electronic conduction, ionic conduction and open porosity for fuel/oxidizer/product ingress and egress. In a method derived from paint formulations, the current technology just uses an empirical blend of catalyst support with attached catalyst and Nafion with sufficient solvent to leave pores when the solvent is removed. The support material forms the scaffold for the pores and must have

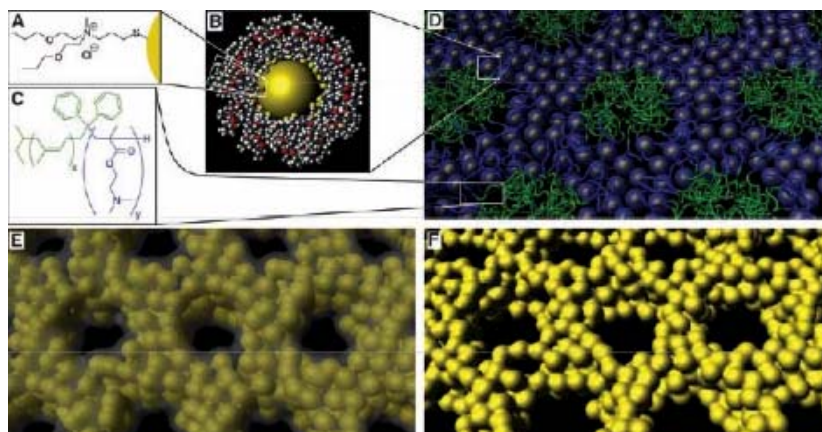


Figure 15

a proper particle morphology and connectivity that is robust enough to do so.

We are applying the structure-directing properties of block co-polymers to determine the chemical systems and processing procedures that will eventually allow the preparation of electrodes in a “one-pot self-assembly process” that could replace the current “paint on” procedure. This is a major challenge indeed. We are approaching this challenge in a step-wise process that first builds in a subset of the required networks and properties, in an effort to learn what chemistries will be able to perform all the desired functions. To build in some of the proper functionalities, we have first exploited di-block copolymers, and have just begun working with tri-block systems that have the potential to form and organize all three percolation networks at once.

We have applied block copolymer structure-directing properties to two classes of materials for fuel cell electrodes: mesoporous metals, e.g., Pt and mesoporous metal oxides, e.g., Nb₂O₅, TiO₂, WO₃. These materials are known to be stable under fuel cell conditions (low pH, applied potential) and can be mesostructured through block copolymers to provide high surface areas with accessible pores (5-50 nm) for the fuel/oxidant to travel to the catalyst nanoparticles. Such materials are synthesized by selectively swelling the hydrophilic block of an amphiphilic block copolymer with hydrophilic nanoparticles of the desired material.

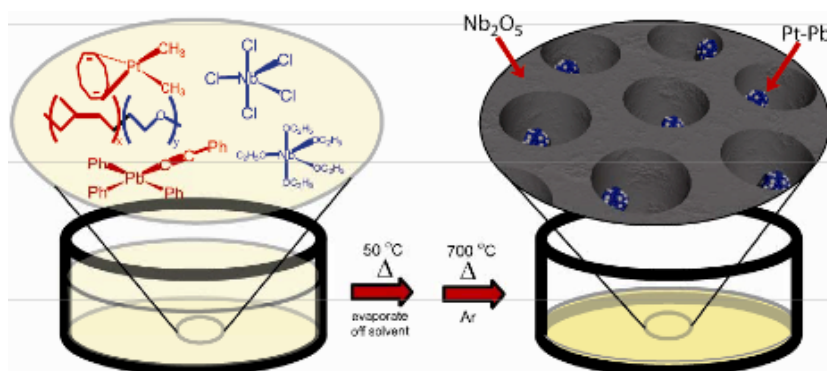


Figure 16

i) Mesoporous Metals. By tuning the ligand design (Fig. 15A), we have successfully made hydrophilic ligand-stabilized Pt nanoparticles (Fig. 15B) that co-assemble with the block copolymer⁷¹ (Fig. 15C) to form metal-rich mesostructured hybrids

with high metal loadings (Fig. 15D). Heat treating this organic-inorganic hybrid under an inert environment (a method developed in our group called the combined assembly by soft and hard chemistries)³⁹ produces an ordered mesoporous Pt-C composite (Fig. 15E).⁷⁴ The carbon is removed through an Ar-O plasma or acid etch to produce an ordered mesoporous Pt mesostructure (Fig. 15F). This material shows promising results for use as the electrocatalyst for hydrogen oxidation in PEMFCs.

Current research and future directions are to extend this work by exploring the design of new ligands for simpler synthesis, making other mesoporous metals for higher cost performance, and to make other ordered morphologies such as bi-continuous structures that may provide even better charge transport and improved fuel accessibility than two-dimensional porous morphologies.

ii) Mesoporous Metal Oxide In a one-pot approach, we can mix in metal oxide precursors and metal catalyst precursors (e.g., Pt and Pb) with the block copolymer to achieve self assembly after evaporation of solvents. Appropriate heat treatment leads to a mesoporous metal oxide structure with the Pt-Pb nanoparticles decorating the walls of the mesopores (Fig. 16).⁴⁹ Formic acid electro-oxidation using this novel material shows four times higher mass activity and lower onset potential than the previously best reported value of PtPb intermetallic nanoparticles supported on carbon.

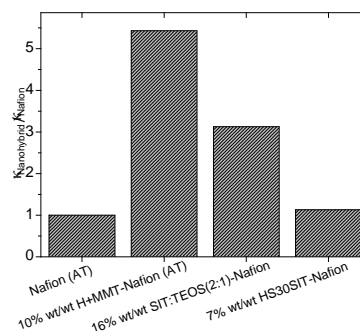


Figure 17. Relative selectivity of Nafion nanocomposite membranes based on clay and silica nanoparticles

Nanocomposite Membranes

An integral part of fuel cells is the electrolyte, whose function is to maximize ionic mobility, while often providing the structural support of the electrodes as well as impeding cross-over of the fuel or any contaminants. A big challenge still facing the scientific community is to engineer an electrolyte material that fulfills the above requirements and that is inexpensive and endures the aggressive fuel cell environment for a long period of time. Furthermore, fuel (hydrogen, methanol, etc.) can permeate the membrane to react at the cathode (so called “cross-over”) without producing electricity and thus lowering the overall efficiency. Crossover

contributes to loss of fuel and generates a mixed potential at the cathode leading to lower overall performance.

We have completed a project that explored nanostructuring as a new design paradigm to synthesize a next generation of fuel cell membranes.^{20,37} Using various inorganic nanoparticles including clay as our nanostructuring elements, we have already demonstrated nanocomposite membranes with dramatically improved performance compared to pure Nafion. Well-dispersed, mechanically robust membranes were prepared by casting from a water suspension at 180°C under pressure. The nanocomposite membranes are much stiffer (by as much as one order of magnitude) and can withstand much higher temperatures; up to 200 °C. In addition, the nanocomposite membranes are much more robust and swell noticeably less in either water or methanol (factor of 10). Lastly, the selectivity (ratio of conductivity over permeability) of nanocomposite membranes is better than that of pure Nafion (Figure 17) by as much as a factor of five. Note that the selectivity of clay based nanocomposites is much better from those based on silica nanoparticles. A small decrease of ionic conductivity for the nanocomposite membranes is more than compensated by the large decrease in methanol permeability.

Small Angle X-ray Scattering profiles reveal a preferential orientation of Nafion chains parallel to the membrane surface, or normal plane (Fig. 18). This preferred orientation is induced by the platy nature of the clay nanoparticles, which tend to align parallel to the surface of the membrane. Orientation is absent in the pure Nafion where the samples appear isotropic. As the concentration of nanoparticles increases, the ionomer peak shifts to higher q values suggesting that the ionic domains compress due to the presence of the nanoparticles.

Nanostructuring is thus a viable approach to dramatically improve the performance of a fuel cell membrane. An outstanding issue, however, is the decrease in ionic conductivity at low relative humidity, RH. The hybrid membranes show the same RH dependence on conductivity as pure Nafion. Since Nafion will have to be replaced to operate at higher temperatures, we will now pursue different directions in our future work. Note, however, that the properties of any ionically conducting polymer membrane can likely be improved by the nanostructuring methods developed in this effort.

Theory:

We have carried out computational studies in an effort to understand, from basic principles, the reactivity and physicochemical properties of the electrocatalytic systems that we have developed. Such continued studies will, in turn, provide valuable insights and clues for the design of better performing, even revolutionary catalyst materials. For example, in order to explain the diminished CO poisoning effects for intermetallic catalysts, we studied the chemisorption of CO on pure Pt and Pt-Pb⁵¹ and Pt-Bi⁴⁷ ordered intermetallic surfaces. Density functional and extended Hückel calculations for Pt-Pb show a lower binding energy of CO on the Pt₃Pb(111) intermetallic surface compared to pure Pt(111)⁵¹ We observe that the filling of the

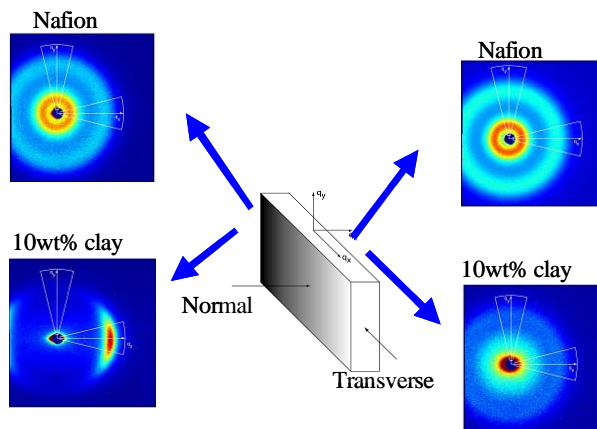


Figure 18. SAXS profiles for Nafion (top) and clay nanocomposite (bottom)

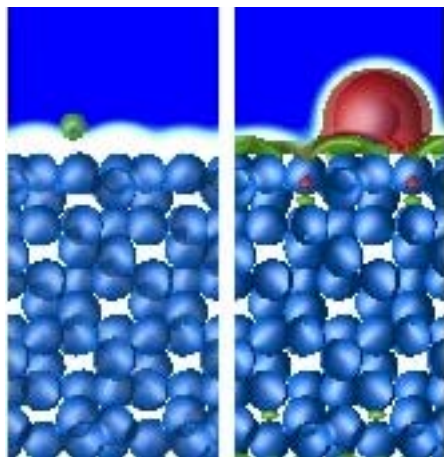


Figure 19. Example of application of JDFT approach described in text: Cr_2O_3 in solution with an adsorbed chloride ion (left panel) and proton (right panel): Cr_2O_3 electron density (light blue surfaces), implicit solvent density (dark blue background), positive and negative induced solvent charges (red and green surfaces, respectively).

high-lying surface Pt orbitals (0001) increases with higher Pb content affecting the Pt-CO interaction when moving from Pt to the Pb-containing intermetallics. Similar effects are observed by extended Hückel calculations for PtBi and PtBi₂ intermetallics.⁴⁷

More recently, we studied the doping of rutile, TiO_2 , with W, because of the potential of the doped material as a stable catalyst support.¹⁸ We find that W-doped TiO_2 is metallic at both high and low doping levels with the W(5d) states dominating the electronic structure near the Fermi level. A Peierls-like distortion leads to pairing of the W atoms in W-rich systems. Lattice parameters match well with the experimental results.

In another study we examined the potential bond-breaking of cyclopropane on the metal surfaces Ti(0001), Cr(110), Fe(110), Co(0001) and Pt(111).²¹ While we did not find C-C bond activation for this strained molecule on any of the metal surfaces, we observed dissociative chemisorption on Ti(0001), not by breaking C-C bonds but through hydrogen abstraction.

On a second front, we have made significant advances¹²¹⁻¹²⁴ addressing the problem that, with standard density-functional methods, realistic electrochemical calculations are not practicable. Such studies are difficult because the random, thermal nature of the solvent environment requires, in principle, the sampling of many configurations of a large number of solvent molecules and ions to properly capture solvation effects. To address this, we have developed a novel *ab initio* approach, the joint density-functional theory (JDFT) method¹²¹⁻¹²², for dealing with solid surfaces in contact with liquid, solvent environments. Figure 24 illustrates the basic concept. The idea is to replace, in a fully rigorous and, in principle, exact way, all of the quantum mechanical and random thermal configurational details of a solvent environment with a relatively simple continuum description, while maintaining a completely first principles description of the system or solute under study. Figure 19 shows the power of this approach to capture screening and chemical solvation effects, showing how chloride ions remain on the oxygen-terminated surface of Cr_2O_3 in contact with a solution whereas hydrous oxide bonds are destabilized by dielectric screening and the protons come off into the solution. The formalism works by extending the combination of Mermin's nonzero temperature¹²⁵ and Capitani's mixed species formulation of density functional theory¹²⁶ to prove that the free energy of a system of nuclei and electrons (i.e., the material surface, including any chemisorbed species) in equilibrium with a solvent environment is given exactly by the following variational principle

$$A = \min_{n(r), N(r,s)} \{F_{\text{KS}}[n(r)] + A_{\text{liq}}[N(r,s)] + U[n(r), N(r,s)]\}$$

where $n(r)$ is the quantum and thermodynamically averaged electron density of the surface at position r , $N(r,s)$ is the likewise averaged density of the nuclei of atomic species s of the solvent at position r , F_{KS} is the traditional electronic-structure Kohn-Sham density functional for the surface or solute under study *while in isolation*, A_{liq} is the so-called "classical" continuum density-functional theory of the solvent system while in isolation, and U is the coupling between

these systems. The key advance is that neither explicit averaging over many random configurations of the solvent molecules needs to be computed nor their electrons included in the calculations, either of which would become extremely demanding computationally. Of course, as mentioned above, when species from the solvent react chemically with the surface, they can always be included in the explicit electronic density-functional theory calculation, as with Cl^- and H^+ in Fig. 19.

We have had great success with this approach and continue to develop it rapidly. In Ref. 121, we showed that a simple combined form for A_{liq} and U , with a single fit parameter, reproduces the solvation energies of a small set of test molecules in pure water to within 0.4 kcal/mol with a computation demand that is only marginally higher (less than a factor of two) than treating the solute in vacuum, and far less demanding than a full quantum and thermodynamic treatment of the solvent. In Ref. 122, we went further and showed that direct approximations to A_{liq} and U can predict solvation energies to again better than 1 kcal/mole, without fitting to any solvation energies whatsoever. More recently, in Ref. 123, we developed the first practical interaction-site density-functional framework for A_{liq} which accounts, *a priori*, for orientational entropy and non-linear dielectric effects in molecular fluids. And, in Ref. 124 we have developed the first density-functional continuum description for liquid water which reproduces the following properties: the dielectric response (nonlocal and nonlinear); the experimental site-site correlation functions among H and O centers; the surface tension; the bulk modulus of the liquid and the variation of this modulus with pressure; the density of the liquid and the vapor phase; and liquid-vapor coexistence. This functional therefore includes, *a priori*, the most important properties of water that are generally added *a posteriori* in the development of continuum models of solvation.

REFERENCES

1. Bell, A. T.; Gates, B. C.; Ray, D., *Basic Research Needs: Catalysts for Energy*. Office of Science, Department of Energy: Washington, D.C., 2007.
2. Hemminger, J.; Fleming, G.; Ratner, M., *Directing Matter and Energy: Five Challenges for Science and the Imagination*. Office of Science, Department of Energy: Washington, D.C., 2007.
3. Lewis, N. L.; Crabtree, G., *Basic Research Needs for Solar Energy Utilization*. Office of Science, Department of Energy: Washington, D.C., 2005.
4. Dresselhaus, M. S.; Crabtree, G.; Buchanan, M., *Basic Research Needs for the Hydrogen Economy*. Office of Science, Department of Energy: Washington, D.C., 2004.
5. Goodenough, J. B.; Abruña, H. D.; Buchanan, M., Report of the Basic Energy Sciences Workshop on Electrical Energy Storage. In US Department of Energy, Office of Basic Energy Sciences: 2007.
6. Dresselhaus, M. S.; Thomas, I. L., Alternative energy technologies. *Nature (London, United Kingdom)* **2001**, 414, (6861), 332-337.
7. Borup, R.; Meyers, J.; Pivovar, B.; Kim, Y. S.; Mukundan, R.; Garland, N.; Myers, D.; Wilson, M.; Garzon, F.; Wood, D.; Zelenay, P.; More, K.; Stroh, K.; Zawodzinski, T.; Boncella, J.; McGrath, J. E.; Inaba, M.; Miyatake, K.; Hori, M.; Ota, K.; Ogumi, Z.; Miyata, S.; Nishikata, A.; Siroma, Z.; Uchimoto, Y.; Yasuda, K.; Kimijima, K.-i.; Iwashita, N.,

- Scientific Aspects of Polymer Electrolyte Fuel Cell Durability and Degradation. *Chemical Reviews (Washington, DC, United States)* **2007**, 107, (10), 3904-3951.
8. Cheng, X.; Shi, Z.; Glass, N.; Zhang, L.; Zhang, J.; Song, D.; Liu, Z.-S.; Wang, H.; Shen, J., A review of PEM hydrogen fuel cell contamination: Impacts, mechanisms, and mitigation. *Journal of Power Sources* **2007**, 165, (2), 739-756.
 9. Gasteiger, H. A., Proton exchange fuel cell materials and R&D needs for future market success. *Electrochemistry (Tokyo, Japan)* **2007**, 75, (2), 103.
 10. Gasteiger, H. A.; Kocha, S. S.; Sompalli, B.; Wagner, F. T., Activity benchmarks and requirements for Pt, Pt-alloy, and non-Pt oxygen reduction catalysts for PEMFCs. *Applied Catalysis, B Environmental* **2005**, 56, (1-2), 9-35.
 11. Mathias, M. F.; Makharia, R.; Gasteiger, H. A.; Conley, J. J.; Fuller, T. J.; Gittleman, C. I.; Kocha, S. S.; Miller, D. P.; Mittelsteadt, C. K.; Xie, T.; Yan, S. G.; Yu, P. T., Two fuel cell cars in every garage? *Electrochemical Society Interface* **2005**, 14, (3), 24-35.
 12. Bagotsky, V. S., *Fuel Cells: Problems and Solutions*. Wiley: New York, 2009.
 13. Larminie, J.; Dicks, A., *Fuel cell systems explained*. 2nd ed.; J. Wiley: Chichester, West Sussex, 2003; p xxii, 406.
 14. Abe, H.; Matsumoto, F.; Alden, L. R.; Warren, S. C.; Abruna, H. D.; DiSalvo, F. J., Electrocatalytic performance of fuel oxidation by Pt₃Ti nanoparticles. *Journal of the American Chemical Society* **2008**, 130, (16), 5452-5458.
 15. Abruna, H. D.; Matsumoto, F.; Cohen, J. L.; Jin, J.; Roychowdhury, C.; Prochaska, M.; van Dover, R. B.; DiSalvo, F. J.; Kiya, Y.; Henderson, J. C.; Hutchison, G. R., Electrochemical energy generation and storage. Fuel cells and lithium-ion batteries. *Bulletin of the Chemical Society of Japan* **2007**, 80, (10), 1843-1855.
 16. Alden, L. R.; Han, D. K.; Matsumoto, F.; Abruna, H. D.; DiSalvo, F. J., Intermetallic PtPb Nanoparticles Prepared by Sodium Naphthalide Reduction of Metal-Organic Precursors: Electrocatalytic Oxidation of Formic Acid. *Chemistry of Materials* **2006**, 18, (23), 5591-5596.
 17. Alden, L. R.; Roychowdhury, C.; Matsumoto, F.; Han, D. K.; Zeldovich, V. B.; Abruna, H. D.; DiSalvo, F. J., Synthesis, Characterization, and Electrocatalytic Activity of PtPb Nanoparticles Prepared by Two Synthetic Approaches. *Langmuir* **2006**, 22, (25), 10465-10471.
 18. Aryanpour, M.; Hoffmann, R.; DiSalvo, F. J., Tungsten-Doped Titanium Dioxide in Rutile Structure; Theoretical Considerations. *Chemistry of Materials* **2009**, 21, (8), 1627-1635.
 19. Blasini, D. R.; Rochefort, D.; Fachini, E.; Alden, L. R.; DiSalvo, F. J.; Cabrera, C. R.; Abruna, H. D., Surface composition of ordered intermetallic compounds PtBi and PtPb. *Surface Science* **2006**, 600, (13), 2670-2680.
 20. Burgaz, E.; Lian, H.; Herrera, R.; Esteves, L.; Giannelis, E. P., Nafion/Clay hybrids with a network structure. *Polymer* **submitted**.
 21. Cahill, T.; Hoffmann, R., Trying to break into the C-C bond of cyclopropane on metal surfaces. **in preparation**.
 22. Casado-Rivera, E. Electrocatalytic activity of ordered intermetallic phases for fuel cell applications. 2006.
 23. Casado-Rivera, E.; Gal, Z.; Angelo, A. C. D.; Lind, C.; DiSalvo, F. J.; Abruna, H. D., Electrocatalytic oxidation of formic acid at an ordered intermetallic PtBi surface. *Chemphyschem* **2003**, 4, (2), 193-199.

24. Casado-Rivera, E.; Volpe, D. J.; Alden, L.; Lind, C.; Downie, C.; Vazquez-Alvarez, T.; Angelo, A. C. D.; DiSalvo, F. J.; Abruna, H. D., Electrocatalytic Activity of Ordered Intermetallic Phases for Fuel Cell Applications. *Journal of the American Chemical Society* **2004**, 126, (12), 4043-4049.
25. Cohen, J. L.; Volpe, D. J.; Abruna, H. D., Electrochemical determination of activation energies for methanol oxidation on polycrystalline platinum in acidic and alkaline electrolytes. *Physical chemistry chemical physics PCCP* **2007**, 9, (1), 49-77.
26. de-los-Santos-Álvarez, N.; Alden, L. R.; Rus, E.; Wang, H.; DiSalvo, F. J.; Abruña, H. D., CO Tolerance Of Ordered Intermetallic Phases. *Journal of Electroanalytical Chemistry* **2009**, 626(1-2), 14-22.
27. DiSalvo, F. J. In *Fuel cells: the final step in a hydrogen economy*, Preprints of Symposia - American Chemical Society, Division of Fuel Chemistry, 2004; 2004; p 241.
28. DiSalvo, F. J., Jr. In *Ordered Intermetallic Catalysts for Fuel Cell Applications*, Abstracts, 35th Northeast Regional Meeting of the American Chemical Society, Binghamton, NY, United States, October 5-7, 2006; 2006; pp NRM-038.
29. DiSalvo, F. J., Jr. In *Synthesis of nanoparticles of ordered intermetallic compounds: The search for improved fuel cell catalysts*, Abstracts of Papers, 233rd ACS National Meeting, Chicago, IL, United States, March 25-29, 2007, 2007; 2007; pp INOR-496.
30. Disalvo, F. J., Jr.; Abruna, H. D. Intermetallic compounds for use as catalysts in fuel cell applications. 2003-US236932004012290, 20030729., 2004.
31. DiSalvo, F. J., Jr.; Abruna, H. D. In *Intermetallic compounds for fuel cell electrocatalysis*, Abstracts of Papers, 226th ACS National Meeting, New York, NY, United States, September 7-11, 2003, 2003; 2003; pp INOR-054.
32. Ghosh, T.; Leonard, B. M.; Zhou, Q.; DiSalvo, F. J., Intermetallic PtZn and Pt₃Zn nanocrystal electrocatalysts synthesized by sodium naphthalide reduction. **in preparation**.
33. Ghosh, T.; Matsumoto, F.; McInnis, J.; Weiss, M.; DiSalvo, F. J.; Abruna, H. D., PtPb nanoparticle electrocatalysts: Control of activity through synthetic methods. *Journal of Nanoparticle Research* **accepted**.
34. Gregoire, J. M.; Kostylev, M.; Tague, M. E.; Mutolo, P. F.; van Dover, R. B.; DiSalvo, F. J.; Abruna, H. D., High-Throughput Evaluation of Dealloyed Pt-Zn Composition-Spread Thin Film for Methanol-Oxidation Catalysis. *Journal of the Electrochemical Society* **2009**, 156, (1), B160-B166.
35. Gregoire, J. M.; Lobovsky, M. B.; Heinz, M. F.; DiSalvo, F. J.; van Dover, R. B., Resputtering phenomena and determination of composition in codeposited films. *Physical Review B Condensed Matter and Materials Physics* **2007**, 76, (19), 195437/1-195437/10.
36. Gregoire, J. M.; van Dover, R. B.; Jin, J.; Disalvo, F. J.; Abruna, H. D., Getter sputtering system for high-throughput fabrication of composition spreads. *The Review of scientific instruments* **2007**, 78, (7), 072212.
37. Herrera, R.; Esteves, L.; Lian, H.; Kellarakis, A.; Giannelis Emmanuel, P., Nafion-Clay nanocomposite membranes: morphology and properties. *Polymer* **submitted**.
38. Jin, J.; Prochaska, M.; Rochefort, D.; Kim, D. K.; Zhuang, L.; DiSalvo, F. J.; van Dover, R. B.; Abruna, H. D., A high-throughput search for direct methanol fuel cell anode electrocatalysts of type Pt_xBi_yPb_z. *Applied Surface Science* **2007**, 254, (3), 653-661.
39. Lee, J.; Orilall, M. C.; Warren, S. C.; Kamperman, M.; DiSalvo, F. J.; Wiesner, U., Direct access to thermally stable and highly crystalline mesoporous transition-metal oxides with uniform pores. *Nature Materials* **2008**, 7, (3), 222-228.

40. Lee, J.; Stefik, M.; Warren, S. C.; DiSalvo, F.; Wiesner, U. In *Nanostructured graphitic carbon/crystalline transition metal oxide composite using a diblock copolymer as a carbon precursor*, Abstracts of Papers, 235th ACS National Meeting, New Orleans, LA, United States, April 6-10, 2008, 2008; 2008; pp PHYS-497.
41. Liu, Y.; Blasini, D. R.; DiSalvo, F. J.; Abruña, H. D., In-situ X-ray grazing incidence diffraction characterization of ordered intermetallic phases for fuel cell applications. **submitted.**
42. Matsumoto, F.; Roychowdhury, C.; Alden, L. R.; DiSalvo, F. J.; Abruña, H., Electrocatalytic Oxidation of Ethanol and Methanol on Ordered Intermetallic Phases in Alkaline Solutions. *Langmuir* **submitted.**
43. Matsumoto, F.; Roychowdhury, C.; DiSalvo, F. J.; Abruna, H. D., Electrocatalytic Activity of Ordered Intermetallic PtPb Nanoparticles Prepared by Borohydride Reduction toward Formic Acid Oxidation. *Journal of the Electrochemical Society* **2008**, 155, (2), B148-B154.
44. Matsumoto, F.; Roychowdhury, C.; Wang, H.; DiSalvo, F. J.; D.", A. H., A Study on the Stability of Electrocatalytic Activity and Tolerance towards Formic Acid Oxidation on Ordered Intermetallic PtPb Nanoparticles. **in preparation.**
45. Miura, A.; Matsumoto, F.; Leonard, B. M.; Abruna, H. D.; DiSalvo, F. J., Synthesis of intermetallic PtZn nanoparticles by reaction of Pt nanoparticles with Zn vapor and their applications as fuel cell catalysts. *Chemistry of Materials* **submitted.**
46. Oana, C. M.; Hoffmann, R.; Abruna, H. D. In *Intermediates involved in the electrocatalytic oxidation of HCOOH on PtBi₂ and PtBi*, Abstracts of Papers, 228th ACS National Meeting, Philadelphia, PA, United States, August 22-26, 2004, 2004; 2004; pp INOR-140.
47. Oana, M.; Hoffmann, R.; Abruna, H. D.; DiSalvo, F. J., Adsorption of CO on PtBi₂ and PtBi surfaces. *Surface Science* **2005**, 574, (1), 1-16.
48. Orilall, M. C.; Abrams, N. M.; Lee, J.; DiSalvo, F. J.; Wiesner, U., Highly crystalline inverse opal transition metal oxides via a combined assembly of soft and hard chemistries. *Journal of the American Chemical Society* **2008**, 130, (28), 8882-+.
49. Orilall, M. C.; Matsumoto, F.; Zhou, Q.; Sai, H.; Abruna, H. D.; DiSalvo, F. J.; Wiesner, U., One-pot synthesis of platinum-based nanoparticles incorporated in mesoporous niobium oxide for next generation fuel cell electrodes. *Chemistry of Materials* **submitted (2009).**
50. Prochaska, M.; Jin, J.; Rochefort, D.; Zhuang, L.; DiSalvo, F. J.; Abruna, H. D.; van Dover, R. B., High throughput screening of electrocatalysts for fuel cell applications. *Review of Scientific Instruments* **2006**, 77, (5), 054104/1-054104/8.
51. Ranjan, C.; Hoffmann, R.; DiSalvo, F. J.; Abruna, H. D., Electronic Effects in CO Chemisorption on Pt-Pb Intermetallic Surfaces: A Theoretical Study. *Journal of Physical Chemistry C* **2007**, 111, (46), 17357-17369.
52. Roychowdhury, C.; DiSalvo, F. J. In *Intermetallic nanoparticles for fuel cell applications: Synthesis and characterization studies*, Abstracts of Papers, 233rd ACS National Meeting, Chicago, IL, United States, March 25-29, 2007, 2007; 2007; pp INOR-630.
53. Roychowdhury, C.; Matsumoto, F.; Mutolo, P. F.; Abruna, H. D.; DiSalvo, F. J., Synthesis, Characterization, and Electrocatalytic Activity of PtBi Nanoparticles Prepared by the Polyol Process. *Chemistry of Materials* **2005**, 17, (23), 5871-5876.
54. Roychowdhury, C.; Matsumoto, F.; Zeldovich, V. B.; Warren, S. C.; Mutolo, P. F.; Ballesteros, M.; Wiesner, U.; Abruna, H. D.; DiSalvo, F. J., Synthesis, Characterization, and Electrocatalytic Activity of PtBi and PtPb Nanoparticles Prepared by Borohydride Reduction in Methanol. *Chemistry of Materials* **2006**, 18, (14), 3365-3372.

55. Sanabria-Chinchilla, J.; Abe, H.; DiSalvo, F. J.; Abruna, H. D., Surface characterization of ordered intermetallic PtBi(001) surfaces by ultra-high vacuum-electrochemistry (UHV-EC). *Surface Science* **2008**, 602, (10), 1830-1836.
56. Sanabria-Chinchilla, J.; Abe, H.; DiSalvo, F. J.; Abruna, H. D., Surface characterization and electrocatalytic activity of ordered intermetallic PtBi(001) surfaces by ultrahigh vacuum-electrochemistry (UHV-EC). *Abstracts of Papers, 235th ACS National Meeting, New Orleans, LA, United States, April 6-10, 2008* **2008**, IEC-149.
57. Smith, S. P. E.; Casado-Rivera, E.; Abruna, H. D., Application of differential electrochemical mass spectrometry to the electrocatalytic oxidation of formic acid at a modified Bi/Pt electrode surface. *Journal of Solid State Electrochemistry* **2003**, 7, (9), 582-587.
58. Stubenrauch, C.; Wielpuetz, T.; Sottmann, T.; Roychowdhury, C.; DiSalvo, F. J., Microemulsions as templates for the synthesis of metallic nanoparticles. *Colloids and Surfaces a-Physicochemical and Engineering Aspects* **2008**, 317, (1-3), 328-338.
59. Tague, M. E.; Jin, J.; Kostylev, M.; Gregoire, J.; Abruna, H. D.; DiSalvo, F. J.; van Dover, R. B.; Prochaska, M. In *High throughput screening methods for fuel cell electrocatalysts*, Abstracts of Papers, 235th ACS National Meeting, New Orleans, LA, United States, April 6-10, 2008, 2008; 2008; pp ANYL-130.
60. van Dover, R. B.; Schneemeyer, L. F., The codeposited composition spread approach to high-throughput discovery/exploration of inorganic materials. *Macromolecular Rapid Communications* **2004**, 25, (1), 150-157.
61. Van Dover, R. B.; Schneemeyer, L. F., The continuous composition spread approach. *Combinational Materials Synthesis* **2003**, 35-68.
62. Volpe, D.; Casado-Rivera, E.; Alden, L.; Lind, C.; Hagerdon, K.; Downie, C.; Korzeniewski, C.; DiSalvo, F. J.; Abruna, H. D., Surface treatment effects on the electrocatalytic activity and characterization of intermetallic phases. *Journal of the Electrochemical Society* **2004**, 151, (7), A971-A977.
63. Volpe, D. J. A paradigm shift: Ordered intermetallic phases as fuel cell electrocatalysts. 2005.
64. Wang, H. S.; Alden, L.; DiSalvo, F. J.; Abruna, H. D., Electrocatalytic mechanism and kinetics of SOMs oxidation on ordered PtPb and PtBi intermetallic compounds: DEMS and FTIRS study. *Physical Chemistry Chemical Physics* **2008**, 10, (25), 3739-3751.
65. Wang, H. S.; Rus, E.; Abruña, H. D., Channel Flow Dual Electrode DEMS Cell: Design and Characterization. **in preparation**.
66. Warren, S.; DiSalvo, F. J.; Wiesner, U., Nanoparticle-tuned assembly and disassembly of mesostructured silica hybrids. [Erratum to document cited in CA146:366518]. *Nature Materials* **2007**, 6, (3), 248.
67. Warren, S. C.; Banholzer, M. J.; Jackson, A. C.; DiSalvo, F. J.; Wiesner, U. B. In *Size-induced demixing of nanoparticles from block copolymers*, Abstracts of Papers, 230th ACS National Meeting, Washington, DC, United States, Aug. 28-Sept. 1, 2005, 2005; 2005; pp PMSE-471.
68. Warren, S. C.; Banholzer, M. J.; Slaughter, L. S.; DiSalvo, F. J.; Wiesner, U. B. In *Inducing flow in solventless metal nanoparticles via ligation of a thiol-containing ionic liquid*, Abstracts of Papers, 232nd ACS National Meeting, San Francisco, CA, United States, Sept. 10-14, 2006, 2006; 2006; pp POLY-591.

69. Warren, S. C.; Banholzer, M. J.; Slaughter, L. S.; Giannelis, E. P.; DiSalvo, F. J.; Wiesner, U. B., Generalized route to metal nanoparticles with liquid behavior. *Journal of the American Chemical Society* **2006**, 128, (37), 12074-12075.
70. Warren, S. C.; DiSalvo, F. J.; Weisner, U. B. Sol-gel precursors and synthesis of functionalized nanostructures. 2007-US780692008031108, 20070910., 2008.
71. Warren, S. C.; DiSalvo, F. J.; Wiesner, U., Nanoparticle-tuned assembly and disassembly of mesostructured silica hybrids. *Nature Materials* **2007**, 6, (2), 156-161.
72. Warren, S. C.; DiSalvo, F. J.; Wiesner, U. B., Morphology control and anisotropic structure formation in mesostructured silica-block copolymer hybrids. *PMSE Preprints* **2006**, 95, 241-242.
73. Warren, S. C.; Jackson, A. C.; Cater-Cyker, Z. D.; DiSalvo, F. J.; Wiesner, U., Nanoparticle synthesis via the photochemical polythiol process. *Journal of the American Chemical Society* **2007**, 129, (33), 10072-3.
74. Warren, S. C.; Messina, L. C.; Slaughter, L. S.; Kamperman, M.; Zhou, Q.; Gruner, S. M.; DiSalvo, F. J.; Wiesner, U., Ordered mesoporous materials from metal nanoparticle-block copolymer self-assembly. *Science* **2008**, 320, (5884), 1748-1752.
75. Warren, S. C.; Perkins, M. R.; DiSalvo, F. J.; Wiesner, U. B., General route to metal-silica-block copolymer mesostructured hybrids with high metal loadings. *PMSE Preprints* **2006**, 95, 380-381.
76. Warren, S. C.; Sai, H.; Mitchell, A. J.; Cater-Cyker, Z. D.; Lee, J.; Gruner, S. M.; DiSalvo, F. J.; Wiesner, U., Thermodynamic versus kinetic control in porous materials from nanoparticle-block copolymer assemblies. *Journal of the American Chemical Society* **submitted**.
77. Wiesner, U.; Warren, S. C.; DiSalvo, F. J. In *Assembly and disassembly of polymer nanoparticle composites*, Abstracts of Papers, 235th ACS National Meeting, New Orleans, LA, United States, April 6-10, 2008, 2008; 2008; pp COLL-342.
78. Woo, N. C.; Ng, B. G.; van Dover, R. B., High-throughput combinatorial study of local stress in thin film composition spreads. *Review of Scientific Instruments* **2007**, 78, (7), 072208/1-072208/5.
79. Xiao, L.; Zhuang, L.; Liu, Y.; Lu, J.; Abruna, H. D., Activating Pd by Morphology Tailoring for Oxygen Reduction. *Journal of the American Chemical Society* **2009**, 131, (2), 602-608.
- 80 (a). Zhang, L.; Xia, D. In *Electro-oxidation of formic acid on ordered intermetallic PtSb*, Fuel Cell and Hydrogen Technologies, Proceedings of the International Symposium on Fuel Cell and Hydrogen Technologies, 1st, Calgary, AB, Canada, Aug. 21-24, 2005, 2005; 2005; pp. 261-269.
- 80 (b). Zhuang, L.; Jin, J.; Abruña, H. D., Direct Observation of Electrocatalytic Synergy. *JACS* **2007**, 129(36), 11033-11035.
- 81(a). Kostalik, H. A.; Robertson, N., J; Clark, T. J.; Coates, G., W, Investigation of Substituent Effects on the Base Stability of Ammonium-Functionalized Polyethylene for Use as Alkaline Anion Exchange Membranes. in preparation.
- 81(b). Robertson, N., J; Clark, T. J.; Kostalik, H. A.; Coates, G., W, Tetraalkylammonium Functionalized Biscyclooctene Monomers Leading to Exceptionally Conductive Alkaline Anion Exchange Membranes. in preparation.
- 81(c). Clark, T. J.; Robertson, N. J.; Kostalik, H. A. I. V.; Lobkovsky, E. B.; Mutolo, P. F.; Abruna, H. D.; Coates, G. W., A Ring-Opening Metathesis Polymerization Route to

- Alkaline Anion Exchange Membranes: Development of Hydroxide-Conducting Thin Films from an Ammonium-Functionalized Monomer. *Journal of the American Chemical Society* **2009**, *131* (36), 12888-12889.
82. Rugolo, J.; Erlebacher, J.; Sieradzki, K., Length scales in alloy dissolution and measurement of absolute interfacial free energy. *Nature Materials* **2006**, *5*, (12), 946-949.
 83. Hayes, J. R.; Hodge, A. M.; Biener, J.; Hamza, A. V.; Sieradzki, K., Monolithic nanoporous copper by dealloying Mn-Cu. *Journal of Materials Research* **2006**, *21*, (10), 2611-2616.
 84. Salgueirino-Maceira, V.; Correa-Duarte, M. A.; Farle, M.; Lopez-Quintela, A.; Sieradzki, K.; Diaz, R., Bifunctional gold-coated magnetic silica spheres. *Chemistry of Materials* **2006**, *18*, (11), 2701-2706.
 85. Thorp, J. C.; Sieradzki, K.; Tang, L.; Crozier, P. A.; Misra, A.; Nastasi, M.; Mitlin, D.; Picraux, S. T., Formation of nanoporous noble metal thin films by electrochemical dealloying of Pt_xSi_{1-x}. *Applied Physics Letters* **2006**, *88*, (3), -.
 86. Erlebacher, J.; Sieradzki, K., Pattern formation during dealloying. *Scripta Materialia* **2003**, *49*, (10), 991-996.
 87. Sieradzki, K.; Dimitrov, N.; Movrin, D.; McCall, C.; Vasiljevic, N.; Erlebacher, J., The dealloying critical potential. *Journal of the Electrochemical Society* **2002**, *149*, (8), B370-B377.
 88. Erlebacher, J.; Aziz, M. J.; Karma, A.; Dimitrov, N.; Sieradzki, K., Evolution of nanoporosity in dealloying. *Nature* **2001**, *410*, (6827), 450-453.
 89. Dimitrov, N.; Mann, J. A.; Vukmirovic, M.; Sieradzki, K., Dealloying of Al₂CuMg in alkaline media. *Journal of the Electrochemical Society* **2000**, *147*, (9), 3283-3285.
 90. Dimitrov, N.; Mann, J. A.; Sieradzki, K., Copper redistribution during corrosion of aluminum alloys. *Journal of the Electrochemical Society* **1999**, *146*, (1), 98-102.
 91. Wagner, K.; Brankovic, S. R.; Dimitrov, N.; Sieradzki, K., Dealloying below the critical potential. *Journal of the Electrochemical Society* **1997**, *144*, (10), 3545-3555.
 92. Sieradzki, K., Curvature Effects in Alloy Dissolution. *Journal of the Electrochemical Society* **1993**, *140*, (10), 2868-2872.
 93. Pourbaix, M., Atlas of Electrochemical Equilibria in Aqueous Solutions. In National Association of Corrosion Engineers: 1974.
 94. Kolen'ko, Y. V.; Burukhin, A. A.; Churagulov, B. R.; Oleinikov, N. N., Phase composition of nanocrystalline titania synthesized under hydrothermal conditions from different titanyl compounds. *Inorganic Materials* **2004**, *40*, (8), 822-828.
 95. Sasaki, K.; Zhang, L.; Adzic, R. R., Niobium oxide-supported platinum ultra-low amount electrocatalysts for oxygen reduction. *Physical Chemistry Chemical Physics* **2008**, *10*, (1), 159-167.
 96. O'Regan, B.; Graetzel, M., A Low-Cost, High-Efficiency Solar-Cell Based on Dye-Sensitized Colloidal TiO₂ Films. *Nature* **1991**, *353*, (6346), 737-740.
 97. Burke, A.; Ito, S.; Snaith, H.; Bach, U.; Kwiakowski, J.; Gratzel, M., The function of a TiO₂ compact layer in dye-sensitized solar cells incorporating "Planar" organic dyes. *Nano Letters* **2008**, *8*, (4), 977-981.
 98. Gerstner, M. E., Examination of the Corrosion Suppression Mechanism on N-Titanium Dioxide Photoanodes. *Journal of the Electrochemical Society* **1979**, *126*, (6), 944-949.
 99. Chang, L. L. Y., Melting Relation in System TiO₂-WO₂. *Journal of the American Ceramic Society* **1968**, *51*, (5), 295-.

100. Chen, G. Y.; Waraksa, C. C.; Cho, H. G.; Macdonald, D. D.; Mallouk, T. E., EIS studies of porous oxygen electrodes with discrete particles - I. Impedance of oxide catalyst supports. *Journal of the Electrochemical Society* **2003**, 150, (9), E423-E428.
101. Colomer, M. T.; Velasco, M. J., Rutile-type dense ceramics fabricated by pressureless sintering of $Ti_{1-x}Ru_xO_2$ powders prepared by sol-gel. *Journal of the European Ceramic Society* **2007**, 27, (6), 2369-2376.
102. Garcia, B. L.; Fuentes, R.; Weidner, J. W., Low-temperature synthesis of a PtRu/Nb_{0.1}Ti_{0.9}O₂ electrocatalyst for methanol oxidation. *Electrochemical and Solid State Letters* **2007**, 10, (7), B108-B110.
103. Horkans, J.; Shafer, M. W., Investigation of Electrochemistry of a Series of Metal Dioxides with Rutile-Type Structure - MoO₂, WO₂, ReO₂, RuO₂, OsO₂, and IrO₂. *Journal of the Electrochemical Society* **1977**, 124, (8), 1202-1207.
104. Murata, Y.; Fukuta, S.; Ishikawa, S., Photoelectrochemical property of rutile (Ti,M)O₂ oxides (M: Nb, Mo, Ta, W) formed on Ti-M binary alloys. *Zairyo to Kankyo* **2000**, 49, 412-419.
105. Pejryd, L., Activity-Composition Relationships of the Solid-Solution (Ti,Mo)O₂ in the Temperature-Range 1350 to 1600 K. *Journal of the American Ceramic Society* **1986**, 69, (9), 717-720.
106. Roy, A.; Dey, S.; Ghose, J., Studies on Ti-W-O system. *Indian Journal of Physics, A* **2000**, 74A, (2), 191-193.
107. Sakata, K.; Nishida, I.; Matsushi, M.; Sakata, T., Electrical and Magnetic Properties of Nb(x)Ti(1-x)O(2). *Journal of the Physical Society of Japan* **1969**, 27, (2), 506-.
108. Smith, J. R.; Walsh, F. C.; Clarke, R. L., Reviews in applied electrochemistry. Number 50 - Electrodes based on Magneli phase titanium oxides: the properties and applications of Ebonex (R) materials. *Journal of Applied Electrochemistry* **1998**, 28, (10), 1021-1033.
109. Chapter 4: The Percolation Model. In *The Physics of Amorphous Solids*, Zallen, R., Ed. John Wiley and Sons: New York, 1983.
110. Ohtomo, A.; Muller, D. A.; Grazul, J. L.; Hwang, H. Y., Artificial charge-modulation in atomic-scale perovskite titanate superlattices. *Nature* **2002**, 419, (6905), 378-380.
111. Kim, J. H.; Ishihara, A.; Mitsushima, S.; Kamiya, N.; Ota, K. I., Catalytic activity of titanium oxide for oxygen reduction reaction as a non-platinum catalyst for PEFC. *Electrochimica Acta* **2007**, 52, (7), 2492-2497.
112. Hayashi, M.; Uemura, H.; Shimanoe, K.; Miura, N.; Yamazoe, N., Reverse micelle assisted dispersion of lanthanum manganite on carbon support for oxygen reduction cathode. *Journal of the Electrochemical Society* **2004**, 151, (1), A158-A163.
113. Liu, Y.; Ishihara, A.; Mitsushima, S.; Kamiya, N.; Ota, K., Zirconium oxide for PEFC cathodes. *Electrochemical and Solid State Letters* **2005**, 8, (8), A400-A402.
114. Limoges, B. R.; Stanis, R. J.; Turner, J. A.; Herring, A. M., Electrocatalyst materials for fuel cells based on the polyoxometalates [PMo(12-n)VnO₄₀]⁽⁽³⁺ⁿ⁾⁻⁾ (n=0-3). *Electrochimica Acta* **2005**, 50, (5), 1169-1179.
115. Kuo, M. C.; Stanis, R. J.; Ferrell, J. R.; Turner, J. A.; Herring, A. M., Electrocatalyst materials for fuel cells based on the polyoxometalates-K-7 or H-7[(P₂W₁₇O₆₁Fe^{III}(H₂O))] and Na(12) or H-12[(P₂W₁₅O₅₆)(₂)Fe-4(III)(H₂O)(₂)]. *Electrochimica Acta* **2007**, 52, (5), 2051-2061.
116. Ushikubo, T., Recent topics of research and development of catalysis by niobium and tantalum oxides. *Catalysis Today* **2000**, 57, (3-4), 331-338.

117. Sun, Z.; Chiu, H. C.; Tseung, A. C. C., Oxygen reduction on teflon bonded Pt/WO₃/C electrode in sulfuric acid. *Electrochemical and Solid State Letters* **2001**, 4, (3), E9-E12.
118. Ribeiro, J.; De Andrade, A. R., Characterization of RuO₂-Ta₂O₅ coated titanium electrode - Microstructure, morphology, and electrochemical investigation. *Journal of the Electrochemical Society* **2004**, 151, (10), D106-D112.
119. Bonakdarpour, A.; Lobel, R.; Sheng, S.; Monchesky, T. L.; Dahn, J. R., Acid stability and oxygen reduction activity of magnetron-sputtered Pt_{1-x}Tax (0 ≤ x ≤ 1) films. *Journal of the Electrochemical Society* **2006**, 153, (12), A2304-A2313.
120. Christian, J. B.; Smith, S. P. E.; Whittingham, M. S.; Abruna, H. D., Tungsten based electrocatalyst for fuel cell applications. *Electrochemistry Communications* **2007**, 9, (8), 2128-2132.
121. Petrosyan, S. A.; Rigos, A. A.; Arias, T. A., Joint density-functional theory: Ab initio study of Cr₂O₃ surface chemistry in solution. *Journal of Physical Chemistry B* **2005**, 109, (32), 15436-15444.
122. Petrosyan, S. A.; Briere, J. F.; Roundy, D.; Arias, T. A., Joint density-functional theory for electronic structure of solvated systems. *Physical Review B* **2007**, 75, (20), -.
123. Lischner, J.; Arias, T. A., Kohn-Sham-Like Approach toward a Classical Density-Functional Theory of Inhomogeneous Polar Molecular Liquids: An Application to Liquid Hydrogen Chloride. *Physical Review Letters* **2008**, 101, (21), -.
124. Lischner, J.; Arias, T. A., Classical density-functional theory of inhomogeneous water including explicit molecular structure and nonlinear dielectric response. *Journal of Physical Chemistry B* submitted.
125. Mermin, N. D., Thermal Properties of Inhomogeneous Electron Gas. *Physical Review* 1965, 137, (5A), 1441-&.
126. Capitani, J. F.; Nalewajski, R. F.; Parr, R. G., Non-Born Oppenheimer Density Functional Theory of Molecular-Systems. *Journal of Chemical Physics* **1982**, 76, (1), 568-573.